Chapter

Graphene Functionalization towards Developing Superior Supercapacitors Performance

Abd Elhamid M. Abd Elhamid, Heba Shawkey, Ahmed A.I. Khalil and Iftitan M. Azzouz

Abstract

Graphene is known as the miracle material of the 21st century for the wide band of participating applications and epic properties. Unlike the CVD monolayer graphene, Reduced graphene oxide (RGO) is a commercial form with mass production accessibility via numerous numbers of methods in preparation and reduction terms. Such RGO form showed exceptional combability in supercapacitors (SCs) where RGO is participated to promote flexibility, lifetime and performance. The chapter will illustrate 4 critical milestones of using graphene derivatives for achieving SC's superior performance. The first is using oxidized graphene (GO) blind with polymer for super dielectric spacer. The other three types are dealing with electrolytic SCs based on RGO. Polyaniline (PANI) was grown on GO for exceptionally stable SCs of 100% retention. Silver decoration of RGO was used for all-solid-state printable device. The solid-state gel electrolyte was developed by adding GO to promote current rating. Finally, laser reduced graphene is presented as a one-step and versatile technique for micropatterning processing. The RGO reduction was demonstrated from a laser GO interaction perspective according to two selected key parameters; wavelength and pulse duration.

Keywords: Polyaniline/RGO, Solid-state, laser-induced graphene, super dielectric spacer, flexible supercapacitor

1. Introduction

Supercapacitors (SCs) are a key block elements in our energy storage perspective that could stand alone or be combined with various types of batteries [1]. Unlike batteries, SCs possess unique features of high power and millions of cycling [2]. Yet, SCs energy density could not match the nowadays batteries [3], the development is focused on extending energy density and engineering flexible devices [2]. The storage mechanism is conducted to the SCs type as following; electric double-layer (EDL), pseudocapacitors and hybrid structure [4]. EDL is the simplest form of storing energy electrostatically due to electrolyte ions, whereas, pseudocapacitors is based on reversible redox reactions through active material's surface resulting in more than 10 times capacitance value than EDL. The hybrid type is combining faradic redox and non-faradic EDL reactions that showing near battery like performance.

Graphene is one of the most discussed electrodes material in energy storage due to outstanding electrical, mechanical and electrochemical performance [4]. Graphene functionalization in SCs is expected to lead the next SCs's generation processing as a result of the following; (i) high surface area of 2630 m^2/g correlated with low theoretical density of 2.28 g/cm^3, (ii) high carrier mobility and electrical conductivity that promote using of graphene as a compact active material/current collector, and (iii) Young's modulus of 1 TPa indicating excellent mechanical strength enabling perfect impeding in flexible and wearable electronics. The easy-to-get graphene form known as reduced graphene oxide (RGO) that is obtained from the reduction of highly oxidized exfoliated graphene oxide (GO). Crude RGO active material suffers from low specific capacitance and restacking over time that minimizes accessible surface area [5]. Therefore, many attempts of adding another material such as conducting polymers, metal oxides and metal NPS were reported [3, 6].

Despite a large number of graphene-based SCs reports, this chapter is focusing on selected milestones on using graphene in SCs according to extensive research work as well as others' reports. Four main points considered graphene derivatives, the first is using graphene oxide/polymer blind as a super dielectric spacer for double layer AC supercapacitor. The other technique is using RGO as efficient nucleation sites for polyaniline (PANI). After that, silver metal NPs decoration/RGO was used to fabricate flexible all-solid-state SCs of high power. Finally, laser-induced graphene is a one-step technique to obtain miniaturized 3D RGO based SCs.

2. Dielectric supercapacitor of pseudo 2D GO

Materials of high dielectric constant are directed for large capacitance circuit element, which enables minimizing dimensions in integrated circuits and basic storage elements, etc. [7–10]. Despite well-known ceramic materials such as Barium titanate-based composites, polymers are low cost and scalable but hold significantly low dielectric response. Thus, nano-composites doped inside a polymer matrix is a promising candidate for promoting dielectric characteristics for wearable and flexible electronics [5]. Among enormous compositions types, RGO and GO are blinded in polymer to expand the dielectric response via two different technique, the first is by forming multiple micro-capacitors inside the spacer while the other is using the oxide function group strong polarization [11]. The present section is revealing the potential of using graphene-based polymer composite potential as a super dielectric spacer for RF SC applications [12].

2.1 Double plate SC of PVA/GO spacer fabrication process

GO suspension of 1 gram in 0.1 L DI water and 8% PVA were used for preparing the mixture. The weight ratio blind was as following: 10%, 20% and 50% of GO to PVA using facile colloidal mixing method at 70°C. The resulted paste was coated on cleaned Al foils strips 0.08 × 40x50 mm^3 to form the compacted spacer. After mild evaporation, the top Al foil was attached to the three different ratios GO/PVA. The double-layer capacitor's spacer thickness was adjected to 475 μm after multiple drying processing using a hot press. The fabricated SCs electric characterization was conducted using LRC meter and multi-channels Potentiostat/Galvanostat. **Figure 1** illustrates a schematic for the whole study steps [12].

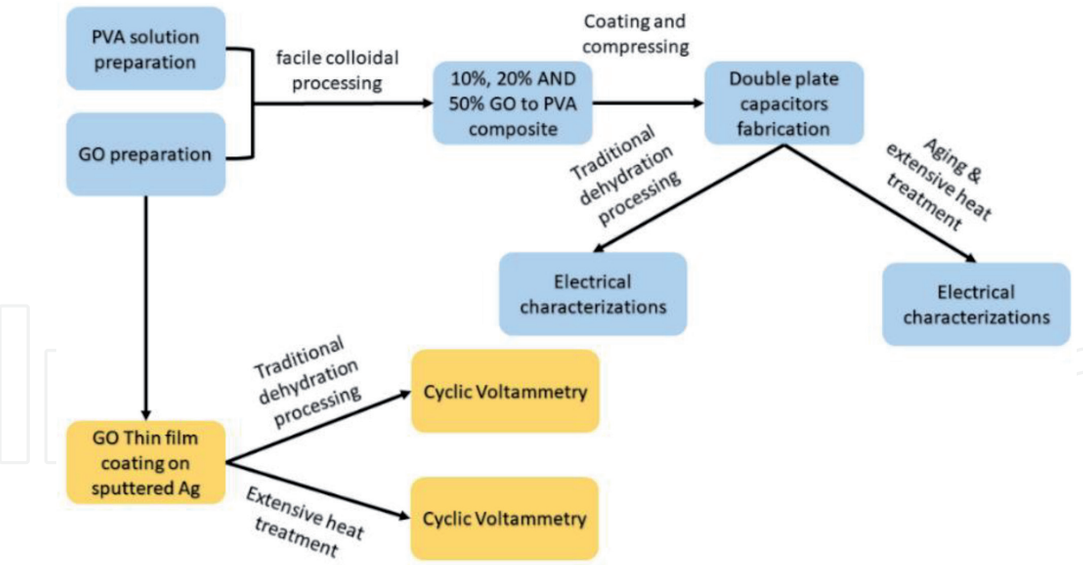

Figure 1.
Schematic of the GO/PVA and GO dielectric spacer study.

2.2 The mega dielectric value of double

The three different double plate capacitors of (10%, 20% and 50%) GO/PVA weight ratio are measured from 20 Hz to 1 MHz, the associated dielectric constants were estimated by knowing area and thickness of the spacers. The whole values are located in the range of mega value (10^6) as showed in **Figure 2(a)**. The dielectric decay over frequency is expected due to weak dipoles response. At low oscillating frequency, the corresponding oxide functionalized groups have the necessary time for alignment correlated with the applied electric field, which will promote the dielectric constant value due to strong polarization. Whereas, the increase in oscillating frequency will eliminate contributed ionic and space charge as well as cause a systematic drop in the dielectric response [13]. Thus, the GO filling inside the PVA polymer matrix achieved high dielectric SC caused by Maxwell- Wagner-Sillar theory [11]. The phase angle in **Figure 2(b)** is an indication of the leakage current through GO/PVA spacers. The higher phase angle than −90 degree resulted from free and bounded charges within the GO/PVA interface. Accordingly, SC's quality factor is linked to the measured phase angle. While the 10% gave the best spacer performance due to low water contents and residuals ions, the 50% ratio showed the lowest dielectric constant as well as quality factor. Low phase angle could be attributed to conductive graphitic defects generated during GO preparation.

The imaginary part (ε″) represents electric field dissipation into heat. The obtained losses could be attributed to GO lattice defects, conductive defects, water contents and ions residuals [13–15]. **Figure 2(c)** present the complex dielectric susceptibility curve (Cole-Cole), where ε is the complex permittivity, ε′ real value and ε″ represent the imaginary part. Several GO oxide functional groups, defects, polymeric chain/GO interface and water molecules will result direct complex time response confirmed by Cole-Cole complex shapes. The 20% GO/PVA based SC cyclic voltammetry is presented in **Figure 2(d)**, which matched the previously measured mega dielectric constant value and performance. Those results indicate balanced filler loading within the polymer matrix of such 20% GO weight value [16]. Finally, the following **Table 1** reports the high dielectric value of using either crude GO or as a polymer matrix filler.

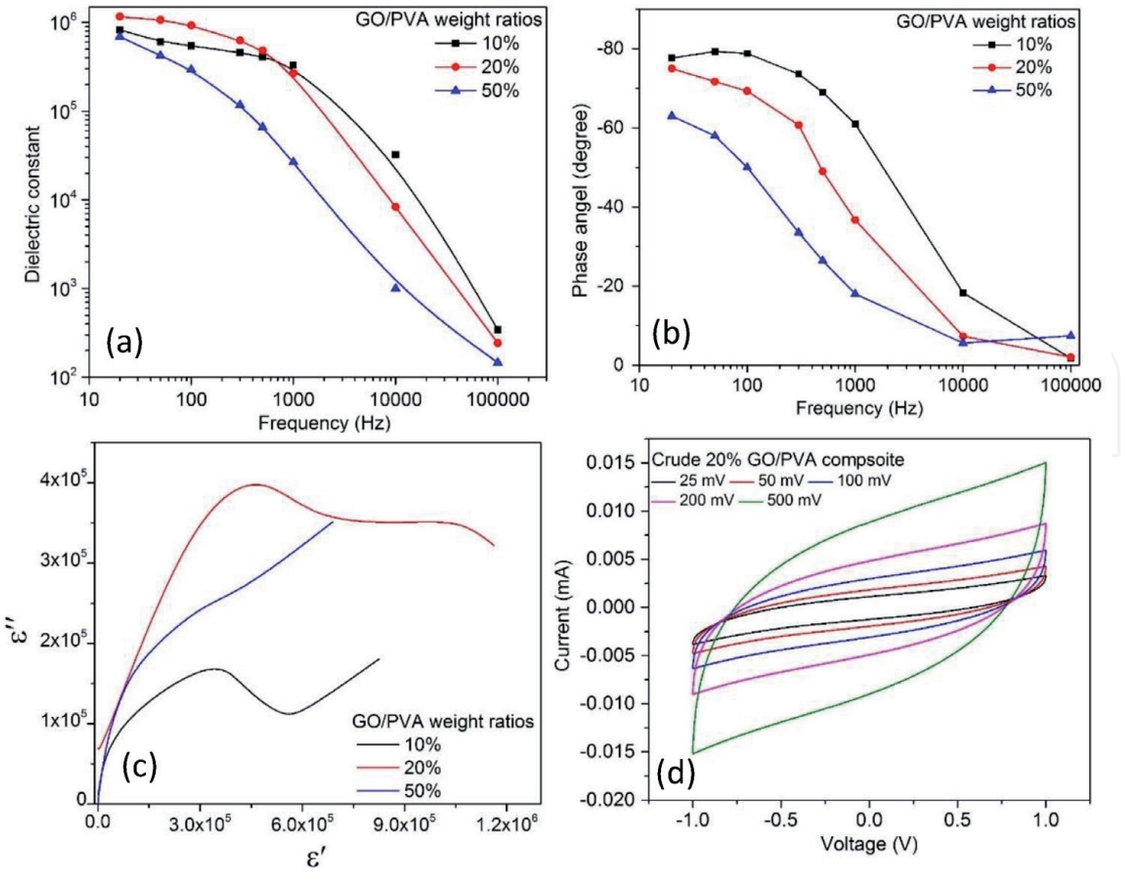

Figure 2.
The three GO/PVA ratio (a) dielectric constants, (b) phase angle, (c) Cole-Cole plot. And (d) the 20% GO/PVA ratio CV at different scan rates. Reproduced with permission from Ref. [12]. Copyright 2021, Elsevier Ltd.

Spacer Materials	DiC value	Reff.
This work (GO) (GO/PVA composite)	10^4 10^6	—
GO/PVA/polyethylene glycol	10^3	[17]
GO/PVA/Polypyrrole	10^3	[16]
GO/PVA/poly (4-styrene sulfonic acid)	10^3	[18]
GO foam	10^2	[14]
GO	pristine (10) annealing (10^3)	[19]
GO hybrid sponges	10^2 to 10^3	[20]
GO	10^4	[15]
GO	10^6	[13]

Table 1.
Dielectric constant of GO-based spacers. Reproduced with permission from Ref. [12]. Copyright 2021, Elsevier Ltd.

3. Conductive polymer graphene composite

3.1 Superior stable PANI reinforced RGO SC

An effective technique to not only prevent RGO restacking but also extend the electrochemical performance is surface composition via polymeric material [21]. PANI, polythiophene and polypyrrole are the most studied conductive

polymers that participated in various application like SC electrodes, sensors, etc. [22]. Among those, PANI is preferable in SC applications due to low cost, controlled conductivity, easy processing and high electrochemical performance [23]. Unfortunately, poor stability is the main drawback. Hence, covalent grafting of PANI with a graphitic based material could promote lifetime, porosity and conductivity [24]. Oxidized graphene function groups are excellent nucleation sites for efficient covalent bonded PANI polymerization. Another advantage of using RGO/PANI composite in SC application is enabling the EDL behavior as well as pseudocapacitance [25].

This section discusses PANI/RGO synthesis via two steps (i) *in situ* polymerization of distilled aniline on GO surface via initially adsorbed Fe^{2+} and (ii) reduction of the composite using hydrazine hydrate. The fabricated symmetric SCs was tested using four different electrolytes namely; sulfuric Acid, phosphoric acid. Potassium hydroxide and sodium sulfate to study the performance over a wide range of transported ions [26].

3.2 Preparation of PANI-RGO SC

2.25 g of Fe_2SO_4 was dissolved in 0.05 L DI water and was drop wised to 0.475 L of GO suspension (10 g/L) while stirred for 2 h. Aniline monomer was double distilled under vacuum for fresh using, and dissolved in 1 M (0.25 L HCl). The Fe_2SO_4 was rabidly added to GO suspension followed by adding Ammonium peroxydisulfate (APS) (4.5 g in 0.25 L 1 M of HCl and was kept stirring overnight at ambient conditions. After collecting and drying, the mixture was dissolved in 1 L DI water followed by sonication for reduction step. Hydrazine hydrate 1:1 to GO weight ratio was added in a boiling water bath. The electrodes PANI/RGO active material was conducted to another polymerization step before collected and drying in vacuum overnight. The paste was prepared by adding 8% PVDF to 92% PANI/RGO then coated 304 Stainless steel foil coated by sputtered 500 nm Pt current collector (sheet resistance is 2 Ω/□). **Figure 3** illustrates SC fabrication and characterization steps schematic [26].

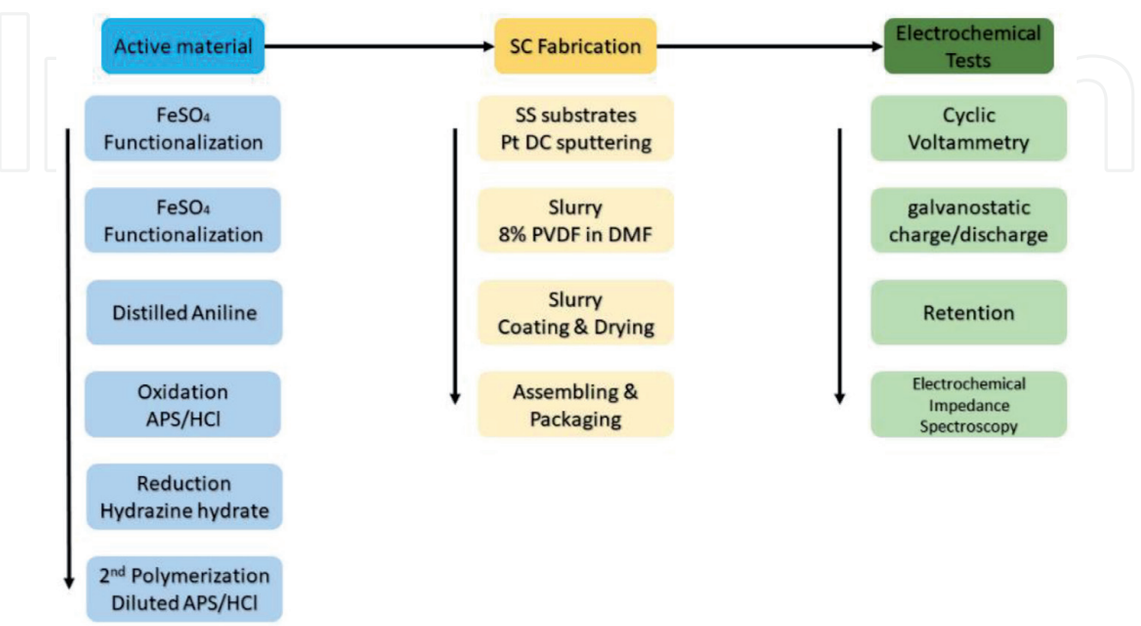

Figure 3.
Schematic of the PANI/RGO based SCs fabrication and measurements.

3.3 Plausible growth mechanism of PANI on RGO

The analysis of PANI polymerization, as well as GO reduction, was confirmed via standard characterization like XRD, Raman & EDX. However, the microscopic imaging is defining a more detailed view of folded RGO and PANI structure. SEM images are presented in **Figure 4(a)** and **(b)** that are showing the high load of PANI completely cover the RGO flakes in thick wood like shape and PANI/RGO flakes, respectively. TEM images illustrate RGO flake folded within dark region **Figure 4(c)**. Whereas, higher magnification TEM image present PANI growth on the RGO surface in tiny islands, which could be attributed to Fe^{2+} sites and GOs' function groups.

Dissociated $FeSO_4$ ions will be functionalized on the dispersed GO flakes. The distilled aniline monomer started to adsorbed on the GO surface [26]. By adding the APS/HCl, Fe (II) will be oxidized to Fe (III) and forming the major oxidation centers and the seed for PANI chains. The applied 1:1 weight ratio between aniline and GO will produce a high load of PANI correlated of high polymerization degree [27]. Fe (II)/APS is promoting effective and rapid polymerization due to direct bonding of the Fe (II) on pseudo-2D GO surface [27]. Thus, APS will react with Fe (II) ions not aniline due to low oxidation potential and produce sulfate radical anions (Eq. (1)) [28]:

$$Fe^{2+} + S_2O_8^{2-} \rightarrow Fe^{3+} + SO_4^{2-} + SO_4^{-\cdot} \quad (1)$$

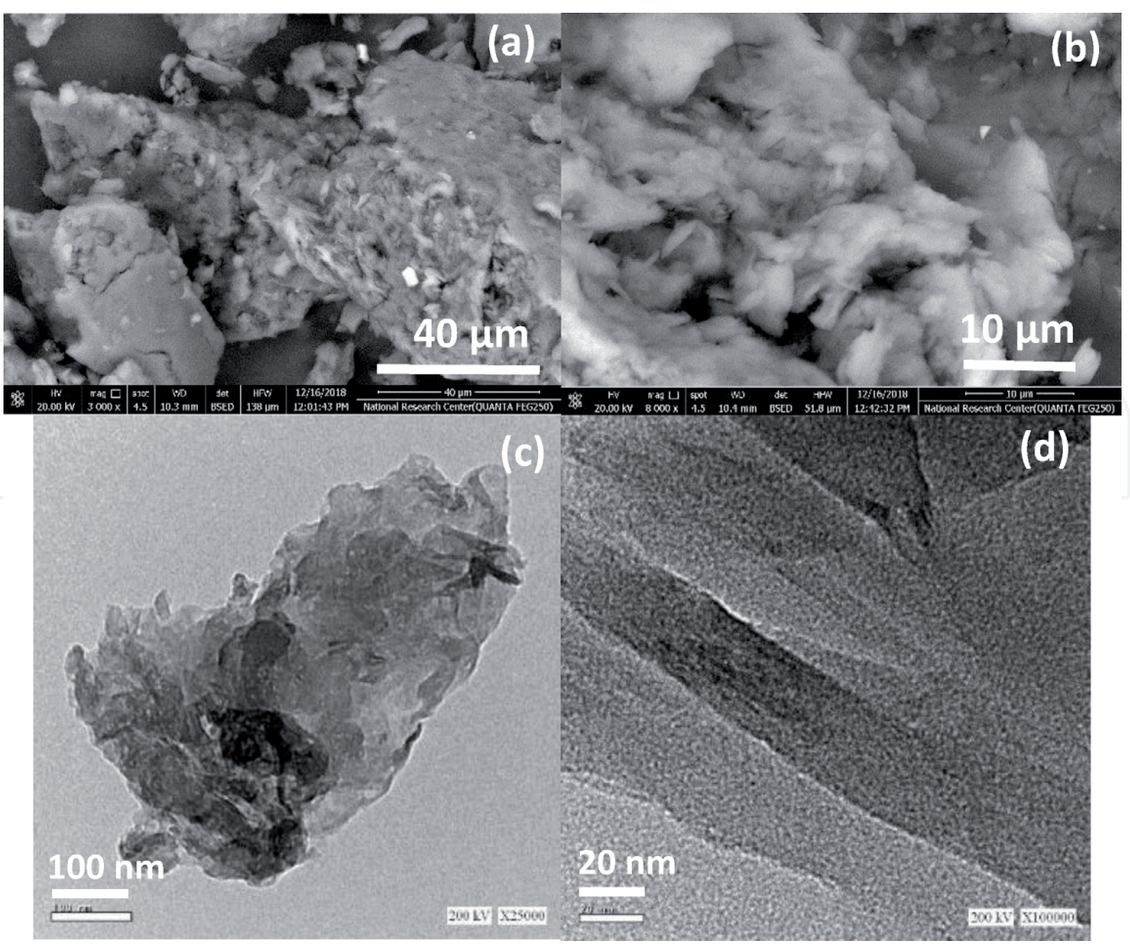

Figure 4.
PANI-RGO at different magnification scale; (a) & (b) SEM images. (c) & (d) TEM images. Reproduced with permission from Ref. [26]. Copyright 2021, Elsevier Ltd.

3.4 Exceptionally stable PANI/RGO SC

The PANI/RGO based SCs were tested in various electrolytes to study the performance of the composite in strong alkaline, strong acid, weak acid and natural medium. Being a time-domain process, galvanostatic charge/discharge test is a

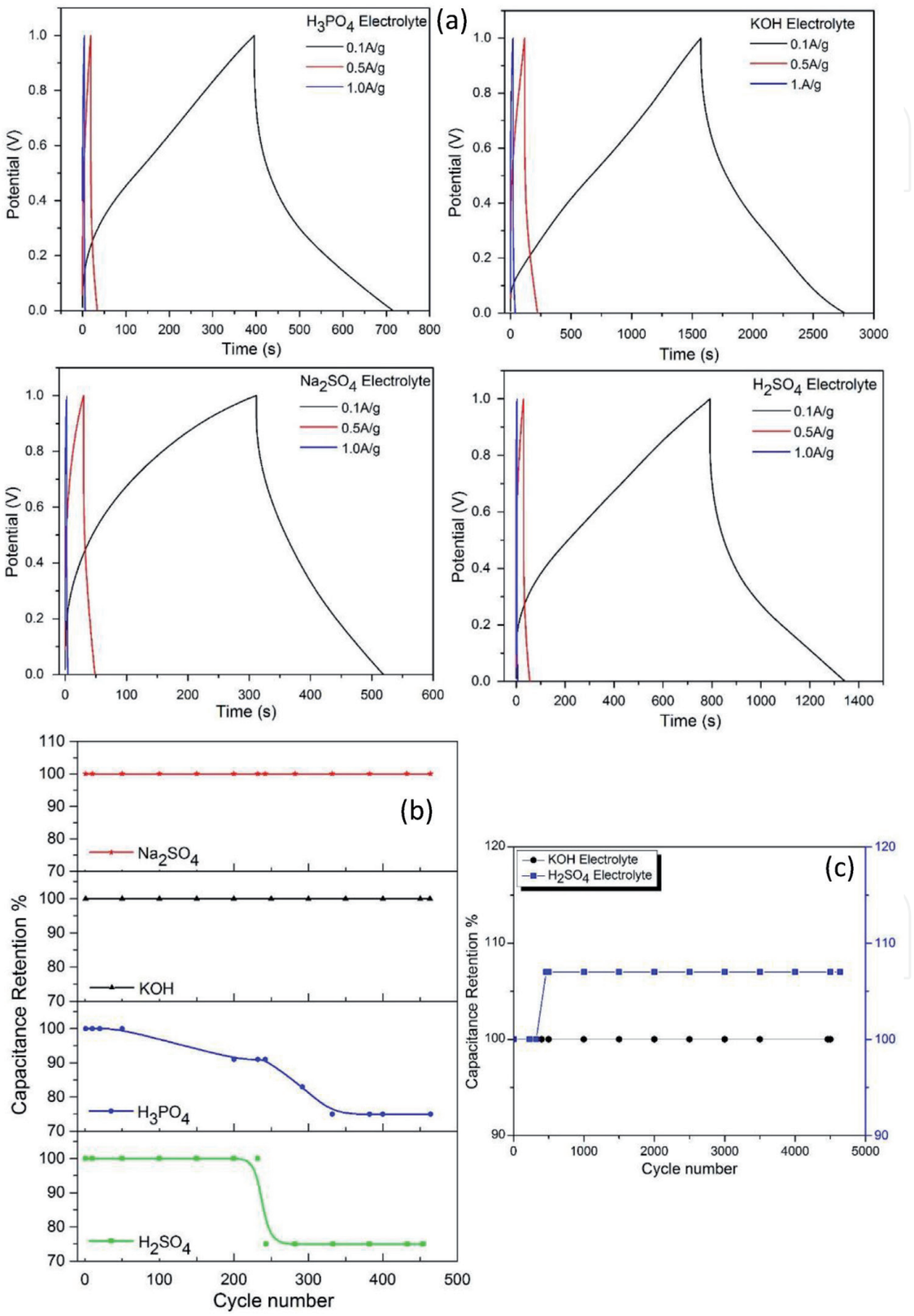

Figure 5.
Different electrolytes, (a) Galvanostatic charge/discharge curves cycle stabilities of different electrolytes. (b) Retention test for 460 cycles at 1A and (c) selected retention for 5000 cycles at 3A. Reproduced with permission from Ref. [26]. Copyright 2021, Elsevier Ltd.

versatile technique of defining specific capacitance, power, energy and lifetime. **Figure 5(a)** presents different electrolyte-based SC at different current. The estimated specific capacitance (0.1A) using H_2SO_4, H_3PO_4, Na_2SO_4 and KOH were 288, 126, 84 and 480 F/g, respectively. The capacitance of the composite could be expanded by using a highly conducting current collector, hot pressing of the active material, using standard cell configuration and a proper separator.

The remarkable result of the prepared PANI/RGO composite is the superior stability in various electrolytes as PANI is degradable at high temperature, high current and charging/discharging process. The first applied retention test at 1A was for nearly 500 cycles **Figure 5(b)**.

The pure EDL performance in alkaline KOH and natural Na_2SO_4 electrolytes present zero decay, whereas, sulfuric and phosphoric show ~75% retention due to aniline doping/degradation during charging. The 5000 cycles (**Figure 5(c)**) are considered to be relatively long cycling for a conducting polymer. The highest obtained capacitive results using H_2SO_4 and KOH were conducted to a 3A/g of current value for more aggressive cycling. Remarkably, KOH based SC maintained the 100% value correlated with the highest achieved capacitance. On the other hand, the sulfuric doping of PANI leads to an increase in the retention value behind 100% [29].

Table 2 presents the obtained results of PANI/RGO concerning others' reports comparatively to clear the role of RGO in enhancing the PANI super capacitive performance. It's worth mentioning that, 3-electrode setup multiplies the actual

Composite material/ Electrolyte	Specific capacitance (F/g)	No. of electrodes configuration	Retention	Process	Ref.
This work 6 M KOH 1 M H_2SO_4 1 M H_3PO_4	565 450 250	2	100% (5000) ~80% (5000) 75% (460)	Non faradic Faradic Non faradic	
PANI/GO/CNTs PVA/H_3PO_4 1 M H_2SO_4	89 729	2 3	80% (5000) 80% (5000)	Non faradic Faradic	[30]
G/PANI 1 M H_2SO_4	790	2	80% (5000)	Faradic	[31]
PANI/G/CNT 1 M H_2SO_4	510	3	91% (5000)	Faradic	[32]
PANI- N doped G/Pd 1 M H_2SO_4	230	2	96% (3000)	Faradic	[33]
PANI/G 1 M H_2SO_4	976	2	89.2% (1000)	Faradic	[34]
G/PANI 1 M H_2SO_4	529	3	85% (1000)	Faradic	[35]
PANI/G 1 M H_2SO_4	413	3	81% (1000)	Faradic	[36]
PANI/Carbon Qds/G 1 M H_2SO_4	871	3	72% (10000)	Faradic	[37]

Table 2.
The PANI-graphene (G) based SCs report. Reproduced with permission from Ref. [26]. Copyright 2021, Elsevier Ltd.

applied voltage that causes a massive increase in measured capacitance of about triple times when compared to the 2-electrode [38]. However, the 2-electrode cell configuration is preferable for practical SCs analysis. The electrochemical stability could be attributed to Fe(II) surface adsorbed on the GO and assisted APS strong locating oxidation.

4. Metal/RGO for solid-state and flexible structure

4.1 Printed devices based on doped graphene

Modern applications of wearable and flexible electronics require a convenient storage device to meet the rapid demands of energy consumption of devices such as ITO sensors and implantable bio-devices [39]. Long lifetime, high power profile, easy manufacturing and eco-friendly structure make the SCs is the best up-to-date candidate for powering such devices [40]. Nevertheless, solid and flexible SCs possess much lower power and energy densities than liquid-based devices that limit the practical coupling with systems. Accordingly, intense research work is applied for promoting the corresponding electrochemical characteristics. The electrodes active materials are already solid but the liquid electrolytes need sophisticated packaging that prevents planer designing. Ionic liquid salts, solid and electrolyte intercalated polymer are different types of the used solid electrolyte. In particular, gel polymer is dissociated ions from acid or base blinded in a polymer matrix. Solid-state gel polymer electrolytes present relatively good ionic conductivity, low cost, high stability, simple principle, reliable, environmentally friendly and safe to handle [41].

This part is using graphene to fabricated flexible, half printed and solid-state SC, the Ag decorated the RGO flakes to prevent restacking. The other functionalization of graphene oxide was for developing the gel polymer to promote high current and scan rate performance [42]. Despite the weak acidic nature of phosphoric acid, it was used as the main ions source inside the GP due to compatibility with RGO and stability over time other than strong acids like sulfuric.

4.2 SCs fabrication procedures

GO suspension was the start material (g/200 mL). Silver nitrate (1 g/50 mL) was added with two different volume ratios 4 ml and 16 ml to a 100 mL of GO suspension, respectively. The two ratios mixture were conducted to Hydrazine hydrate as a strong reduction agent and will be known as sample 1 (4 ml $AgNO_3$) while sample 2 (16 ml $AgNO_3$). The developed gel polymer was performed by dissolving 10% PVA at first and adding an equal weight of phosphoric acid. Finally, GO and PANI of weight 0.03 and 0.01 g were added to the GP, respectively.

A handmade plastic mask was used to make Ag/RGO electrode of dimensions 1x4 cm^2 (0.1 g) using doctor blade. After drying, the GP was coated followed by the second electrode. Lastly, the two devices were peeled off and a metal contact was sputtered on both sides. The schematic in **Figure 6**. illustrates devices fabrication procedures and applied electrochemical measurements [42].

4.3 The remarkable obtained printed SCs performance

TEM image in **Figure 7**. illustrates GO, RGO and Ag-doped RGO, respectively. The folded GO single layer is a clear sheet and the reduction of RGO make defects

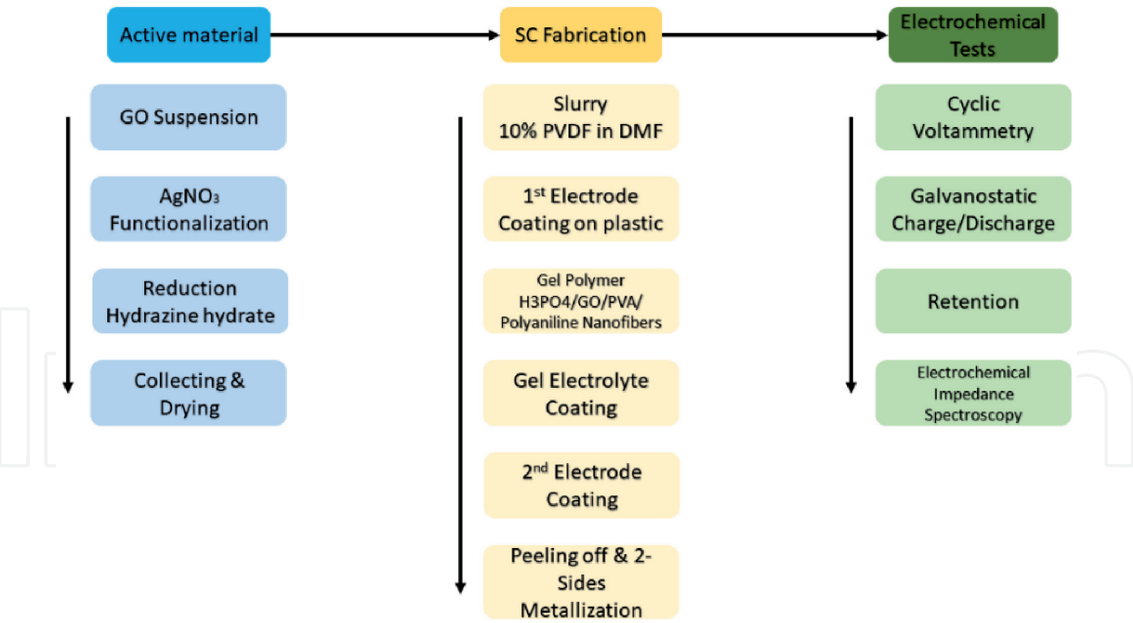

Figure 6.
Schematic of the Ag/RGO flexible SCs fabrication and measurements.

and multilayer represented by the dark regions. However, the silver nanoparticles incorporated RGO could be observed in the dark spots, the RGO do not present the dark defects and multilayered restacked shape due to the intercalated Ag particles. Thus, the as-prepared active material of Ag/RGO will show higher surface area, stability and conductivity. **Figure 7(d)** presents a captured image of the multi-layers printed symmetric SC on the support plastic film. And **Figure 7(e)** represents SC after peeling-off and current collectors metalization. Silver was used for met-alization to reduce mismatch and reduce sheet resistance. The fabricated SCs were stretchable and flexible.

The Ag/RGO SCs was tested at a relatively high current value of 2A/g for a solid-state device by applying galvanostatic cycling. **Figure 8** shows the first three cycles where the time scale of sample 2 is nearly four-fold than sample 1 based SC. Sample 1 is located within the millisecond range, which confirms Ag doping ratio impact on such solid-state SC capacitive value. **Table 3** incorporates the estimated specific capacitance results of sample 1 and 2 via measured cycling voltammetry which is in good agreement with galvanostatic cycling results.

The electrochemical impedance spectroscopy is playing a key role in defin-ing the solid electrolyte performance, the measurement was performed at a wide range from 0.1 Hz to 2 MHz **Figure 8(b)**. Nyquist plot and equivalent circuit measurements were obtained using VSP300 EC-Lab., the matched equivalent circuit is [R1 + C1/(R2 + Q2/(R3 + W3))], Q2 a constant phase element as a time-constant distribution function. R1 charge transfer resistance within electrodes. The low resistance region slop behavior is due to phosphoric weak acid natural [43]. Electrode/electrolyte interface is some sort of a junction represented by a small signal response equivalent circuit. The resistance originated from the charge transfer across such interfacial potential barrier besides electrolyte internal ohmic resistance. At extremely low frequency, the charge transfer resistance is polariza-tion resistance. Whereas, the high frequency will reduce the resistance till reaching R1 value. R2 and R3 are the resistance of (silver current collector+ Ag/RGO active material+ metal/active material Interface contact). They are not equal as the peeling off cause roughness of one surface over the other that modified contact points and

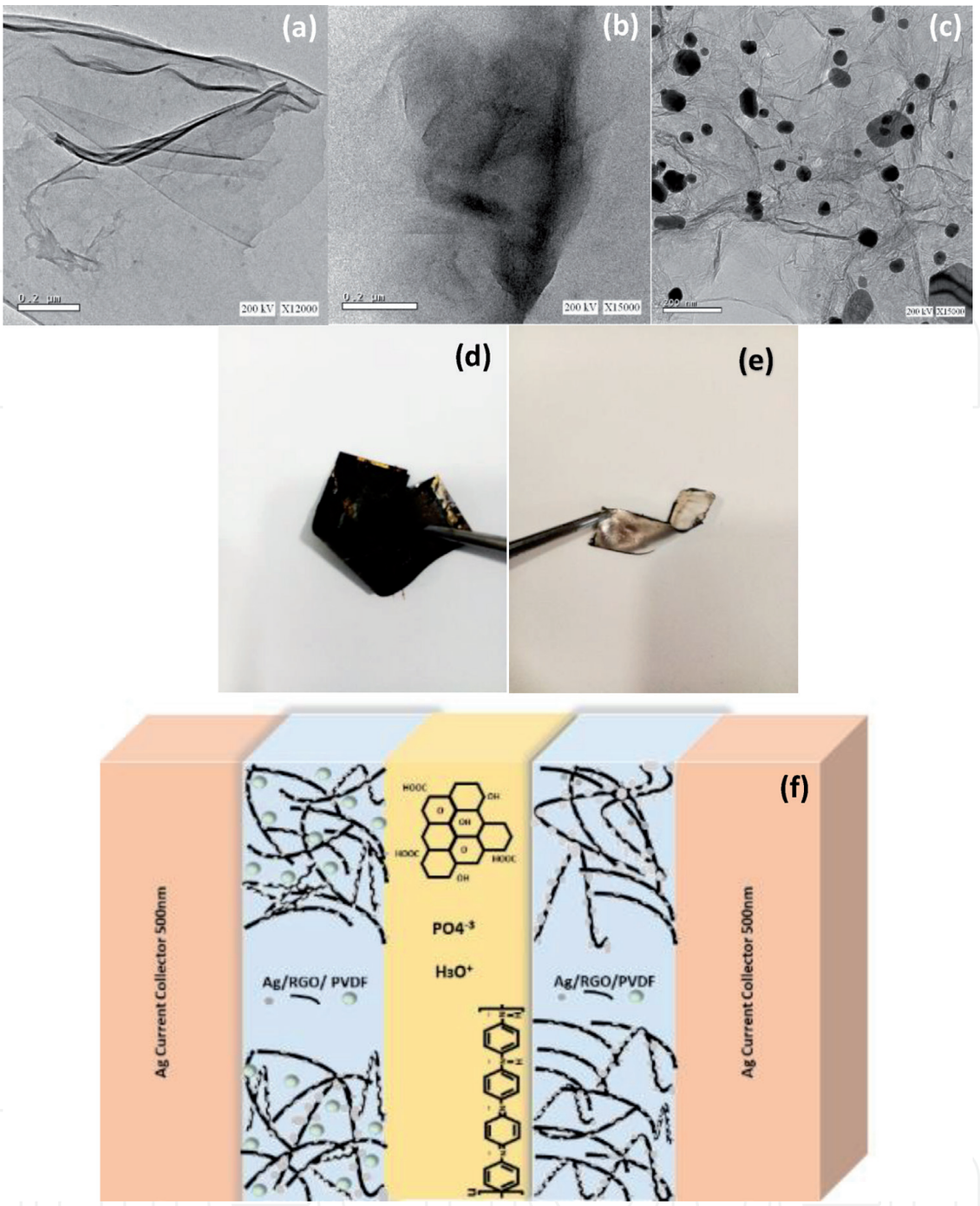

Figure 7.
TEM images of GO, RGO and Ag/RGO. Digital images of the flexible SCs. (d) on a plastic substrate. (e) after peeling and silver coating. (f) Final SC structure. Reproduced with permission from Ref. [42]. Copyright 2021, IEEE.

induced structural defects. During SC charging/discharging, Warburg impedance (W3) represnts semi-infinite one direction liner diffusion of electrolytic ions. The C1 is the magnitude of the two electrodes capacitance. The equivalent series resistance of sample 1 and sample 2 were 2.9 and 0.5317 ohms, respectively. Despite the obtained relatively small ESR for a solid-state SC, it could be further enhanced by the following; (i) using a high mobility ions based electrolyte, (ii) using a strong electrolyte, (iii) full printed structure using metallic ink as plasma deposition induce defects and (iv) applying layer by layer systematic hot compression and vaccum drying.

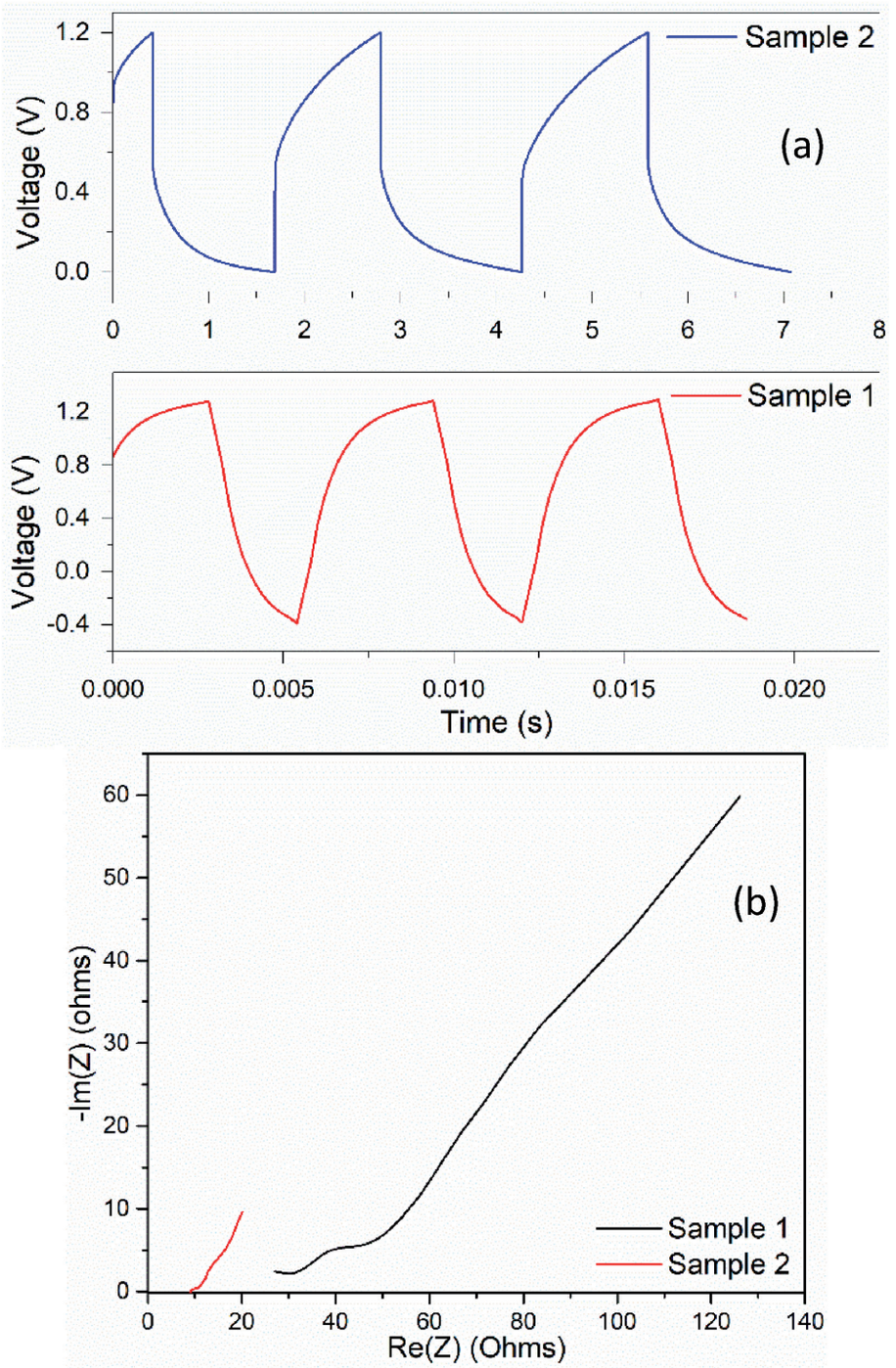

Figure 8.
(a) Charging/discharging test at 2A/g. (b) EIS test. Reproduced with permission from Ref. [42]. Copyright 2021, IEEE.

Scan rates	Sample 1	Sample 2
10 mv/sec	37.5 F/g	164 F/g
20 mv/sec	20 F/g	96.6 F/g
50 mv/sec	10 F/g	51.3 F/g
100 mv/sec	6 F/g	31.57 F/g
200 mv/sec	4.5 F/g	19.24 F/g

Table 3.
Estimated specific capacitance at different scan rates. Reproduced with permission from Ref. [42]. Copyright 2021, IEEE.

5. Laser-assisted RGO SC fabrication

5.1 3D RGO SC with laser irradiation

Conventional SCs are obeying two main configurations, the first is parallel plates and in-between a dielectric separator, the other is three parallel plates and in-between two dielectric separators to form two parallel-connected identical SCs. Those two designs are using a 3D structure and not convenient for planer, compact and miniaturized applications [44]. The developed IDE designs into interdigitated pattering of controlled dimensions will show diverse features over the conventional structure such as [45]; (i) fabrication on-plane macro/micro/nano in-plan SC, (ii) fast sidelong ions transportation, (iii) terminate separator usage and (iv) high power/energy due to confinement of electric field. For creating such fingers patterns SC, lithography techniques are used as it's a matter of certain dimensions etching processing. Photolithography, screen printing, laser dry etching and lift-off processing are used to fabricate complicated SCs designs [46]. However, most of SCs active material will

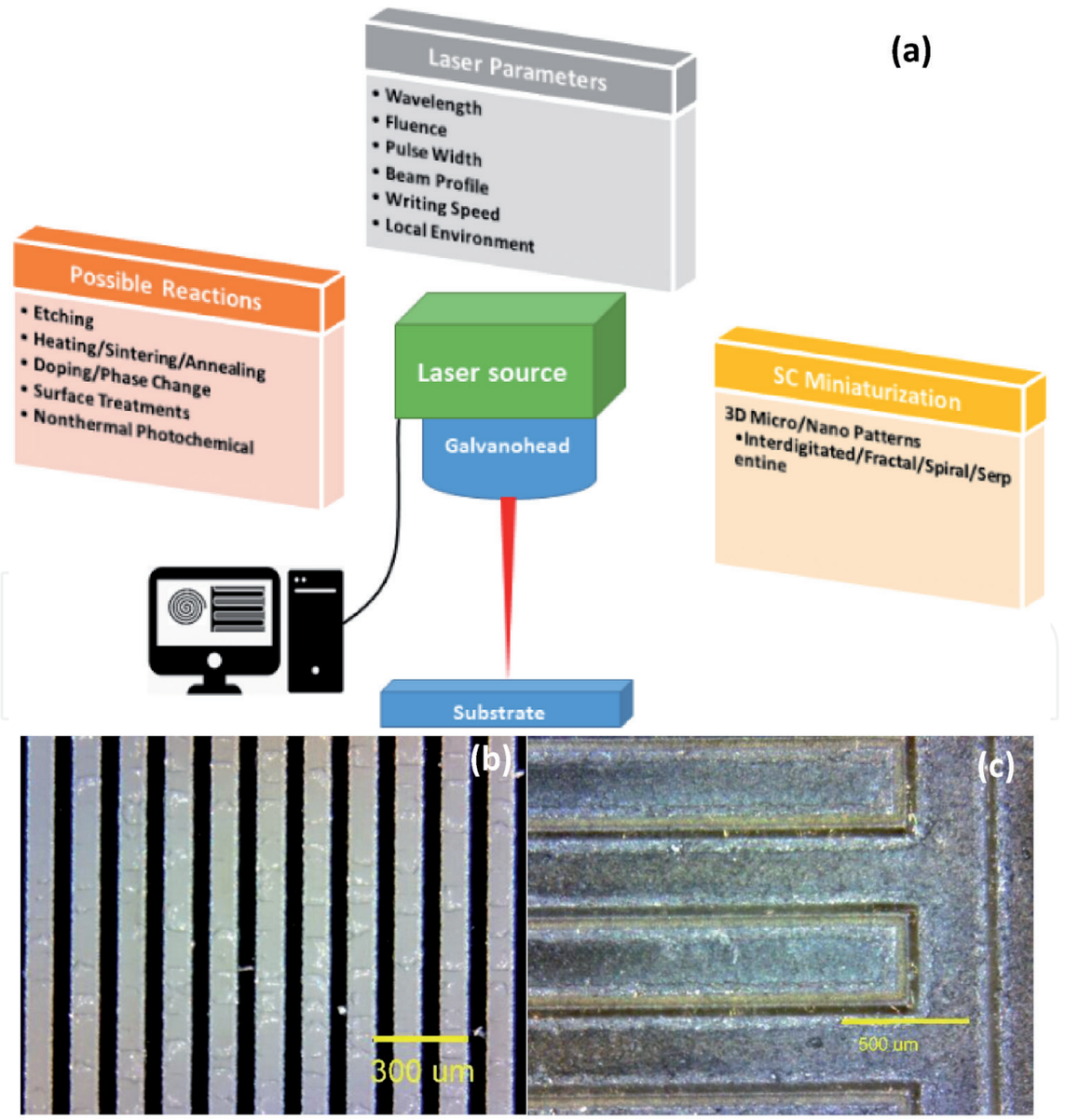

Figure 9.
(a) LDWT setup for SC patterning process. (b) and (c) microscopic images of ongoing using a nanosecond laser in micro SCs processing.

be affected by exposure to chemicals and multi-processing steps which will not match the easy-to-fabricated principle. Thus, laser processing can apply etching as well as controlled structure modification via laser material interaction.

GO is perfect a starting material for laser processing. Dispersion could be functionalized with various nanoparticles and deposited directly on substrates via liquid-phase processing [47]. The concept of using RGO as a commercial source of graphene especially in electronics applications is to reduce the oxygen groups to a highly conductive 2D layered structure. The previously mentioned flexible and PANI/RGO SC are conducted to chemical reduction techniques. However, there are various reduction techniques such as; thermal annealing, microwave flash reduction, laser-assisted processing and high-density UV reduction that affect the resulted RGO characteristics [48]. One of the effective techniques to reduce the dielectric GO into 3D network RGO for SC applications is laser direct writing

Laser	Description	Advantages	Drawbacks
CW CO_2 10600 nm	The most used laser in industry like cutting and welding. It can deliver direct heating to the GO film or carbonize polymer to obtain carbon like graphene Kapton.	• A relatively cheap laser system. • In vacuum or pure inert gas Ar/N_2 will promotes highly conductive RGO with an excellent degree of graphitization. • Mass production technique.	• Cannot apply etching or high precision patterning. • Complex multi-layer SC processing will not be affordable as there will be multi heat conduction constants and melting points. • Local heating will induce RGO defects.
CW 780, 788, 790 nm	It's one of the first trials in applying one-step GO reduction patterning at ambient conditions using CD lightscribe.	• Easy, cheap and results fair reduction.	• No control of power. • Cannot apply etching or high precision pattering. • Continuous beam induces RGO defects.
Pulsed nanosecond 1064/532/248 nm	This laser offers about Megawatt peak power which offers a unique interaction. Two main GO reduction process is working alternatively in major and minor possibility depend on the wavelength.	• Achieve reduction as well as etching processing of complex designs. • Fiber lasers enable mass production. • Could apply both photo (chemical/thermal) GO reduction.	• The thermal energy is propagating during etching within generating heat affected zone and affect the patterning precision.
Pulsed Femtosecond 800 nm	The Ultrafast laser is famous for cold nonthermal processing and pattering blow the diffraction limits.	• The generated pattern craters will be clean with well-defined edges. • Ability to create several nanometers pattern and spacing SC in just one step.	• The strong cold processing in not effective in restoring graphene-like structure and related electric properties.

Table 4.
Different laser type for SCs fabrication process.

technique (LDWT) that enables fast, low cost, easy-processing and maskless patterning [46]. Laser processing of SCs is accessible for most of available rigid and flexible substrates.

5.2 LDWT of RGO based miniaturized SC

Figure 9 presents the LDWT processing main parameters that affect the resulted SC performance. Many reports discuss the corresponding laser parameters, interactions and resulted RGO characteristics [49, 50]. During laser processing, GO reduction is governed by photothermal oxide group removal and photochemical bond breaking. Laser wavelength and pulse duration are the two main key parameters of SC processing. The laser wavelength controls the major photoreduction process of being photochemical ($\leq$ 400 nm) or photothermal ($\geq$ 400 nm).

photochemical process is directly conducted to photon energy that can break oxygen functional groups. The photothermal process is focused on near-infrared region and infrared bands. The deposited thermal energy on GO is maximized upon increasing the beam density to induce local heating within a certain heat-affected zone. This sort of heat can break oxygen radicals as well. In addition, long wavelengths of fast/ultrafast pulse duration could apply photochemical reduction through nonlinear processes and multiphoton absorption [51]. **Table 4** is concluding the GO reduction process using most common laser sources [52–54].

6. Conclusions

Finally, graphene not only proved effective participation in different types of SCs but showing superior electrochemical and electromagnetic performance. PVA/GO composite could work as an efficient super dielectric spacer of mega value 10^6 thanks to the intercalated water dipoles and oxide functional groups. Maxwell- Wagner- Sillar effect expanded the PVA blind dielectric response. By using Fe(II) as a growth mediated oxidizer for PANI growth on GO surface, 100% retention at high current after 5000 cycles at 3A/g was obtained. The PANI/RGO showed EDL performance for H_3PO4, Na_2SO_4 and KOH. For a flexible and printed SC fabrication, silver doped RGO has 29.5 Wh/Kg energy at 2A. The high current rating was promoted via GO impeding inside the electrolytic solid polymer matrix. The miniaturization of one-step fabricated SC is using laser-assisted reduction technique. The CO_2 is a cost-effective direct heating source that induces thermal reduction, whereas, a femtosecond laser is using cold processing that reduces the oxide groups but with a low degree of graphenezation. Nanosecond laser sources combine thermal and photochemical reduction through the GO film.

Conflict of interest

We declare no conflict of interest.

Author details

Abd Elhamid M. Abd Elhamid[1,2*], Heba Shawkey[3], Ahmed A.I. Khalil[1] and Iftitan M. Azzouz[1]

1 Laser Sciences and Interactions Department, National Institute of Laser Enhanced Sciences (NILES), Cairo University, Giza, Egypt

2 Nanotechnology Laboratory, Electronics Research Institute, El Nozha, Egypt

3 Microelectronics Department, Electronics Research Institute, El Nozha, Egypt

*Address all correspondence to: a.m.abdelhamid@eri.sci.eg

References

[1] Capasso C, Veneri O. Integration between Super-capacitors and ZEBRA Batteries as High Performance Hybrid Storage System for Electric Vehicles. Energy Procedia. 2017;105:2539-44. DOI: 10.1016/j.egypro.2017.03.727

[2] Huang S, Zhu X, Sarkar S, Zhao Y. Challenges and opportunities for supercapacitors. APL Mater. 2019;7. DOI: 10.1063/1.5116146

[3] Majumdar D, Mandal M, Bhattacharya SK. Journey from supercapacitors to supercapatteries: recent advancements in electrochemical energy storage systems. Emergent Mater. 2020;3:347-67.

[4] Banerjee S, Sinha P, Verma KD, Pal T, De B, Cherusseri J, et al. Capacitor to Supercapacitor BT - Handbook of Nanocomposite Supercapacitor Materials I: Characteristics. In: Kar KK, editor. Cham: Springer International Publishing; 2020. p. 53-89. DOI: 10.1007/978-3-030-43009-2_2

[5] El-Gendy DM, Ghany NA, El Sherbini EF, Allam NK. Adenine-functionalized Spongy Graphene for Green and High-Performance Supercapacitors. Sci Rep. 2017;7:1-10. DOI: 10.1038/srep43104

[6] Li Q, Horn M, Wang Y, MacLeod J, Motta N, Liu J. A review of supercapacitors based on graphene and redox-active organic materials. Materials; 2019;12: 703. DOI: 10.3390/ma12050703

[7] Lu CY, Chang-Liao KS, Lu CC, Tsai PH, Kyi YY, Wang TK. Investigation of voltage-swing effect and trap generation in high-k gate dielectric of MOS devices by charge-pumping measurement. Microelectron Eng. 2008;85:20-6. DOI: 10.1016/j.mee.2007.02.012

[8] Wilk RW. High dielectric constant materials. In: Gilmer, D. Huff HR, editors. Springer; 2005. 707 p. DOI: 10.1007/b137574

[9] Behera P, Ravi S. Effect of Ni doping on structural, magnetic and dielectric properties of M-type barium hexaferrite. Solid State Sci. 2019;89:139-149. DOI: 10.1016/j.solidstatesciences.2019.01.003

[10] Das R, Choudhary RP. Studies of structural, dielectric relaxor and electrical characteristics of lead-free double Perovskite: Gd2NiMnO6. Solid State Sci. 2019;87:1-8. DOI: 10.1016/j.solidstatesciences.2018.10.020

[11] Wadhwa H, Kandhol G, Deshpande UP, Mahendia S, Kumar S. Thermal stability and dielectric relaxation behavior of in situ prepared poly(vinyl alcohol) (PVA)-reduced graphene oxide (RGO) composites. Colloid Polym Sci. 2020;298:1319-33. DOI: 10.1007/s00396-020-04718-0

[12] Abd Elhamid AM, Shawkey H, Nada AA, Bechelany M. Anomalous dielectric constant value of graphene oxide/Polyvinyl alcohol thin film. Solid State Sci. 2019;94:28-34.

[13] Kumar KS, Pittala S, Sanyadanam S, Paik P. A new single/few-layered graphene oxide with a high dielectric constant of 106: contribution of defects and functional groups. RSC Adv. 2015;5:14768-79. DOI: 10.1039/C4RA10800K

[14] Hou ZL, Liu X Da, Song WL, Fang HM, Bi S. Graphene oxide foams: the simplest carbon-air prototypes for unique variable dielectrics. J Mater Chem C. 2017;5:3397-407. DOI: 10.1039/c6tc04971k

[15] Liu J, Galpaya D, Notarianni M, Yan C, Motta N. Graphene-based thin

film supercapacitor with graphene oxide as dielectric spacer. Appl Phys Lett. 2013;103:1-5. DOI: 10.1063/1.4818337

[16] Deshmukh K, Ahamed MB, Pasha SKK, Deshmukh RR, Bhagat PR. Highly dispersible graphene oxide reinforced polypyrrole/polyvinyl alcohol blend nanocomposites with high dielectric constant and low dielectric loss. RSC Adv. 2015;5:61933-45. DOI: 10.1039/C5RA11242G

[17] Deshmukh K, Ahamed MB, Sadasivuni KK, Ponnamma D, Deshmukh RR, Pasha SKK, et al. Graphene oxide reinforced polyvinyl alcohol/polyethylene glycol blend composites as high-performance dielectric material. J Polym Res. 2016;23:159. DOI: 10.1007/s10965-016-1056-8

[18] Deshmukh K, Ahamed MB, Sadasivuni KK, Ponnamma D, AlMaadeed MAA, Khadheer Pasha SK, et al. Graphene oxide reinforced poly (4-styrenesulfonic acid)/polyvinyl alcohol blend composites with enhanced dielectric properties for portable and flexible electronics. Mater Chem Phys. 2017;186:188-201. DOI: 10.1016/j.matchemphys.2016.10.044

[19] Kavinkumar T, Sastikumar D, Manivannan S. Effect of functional groups on dielectric, optical gas sensing properties of graphene oxide and reduced graphene oxide at room temperature. RSC Adv. 2015;5:10816-25. DOI: 10.1039/C4RA12766H

[20] Wang Y, Zhang KL, Zhang BX, Ma CJ, Song WL, Hou ZL, et al. Smart mechano-hydro-dielectric coupled hybrid sponges for multifunctional sensors. Sensors Actuators, B Chem. 2018;270:239-46. DOI: 10.1016/j.snb.2018.05.023

[21] Radhakrishnan S, Kim SJ. Facile fabrication of NiS and a reduced graphene oxide hybrid film for nonenzymatic detection of glucose. RSC Adv. 2015;5:44346-52. DOI: 10.1039/c5ra01074h

[22] Guo X, Facchetti A. The journey of conducting polymers from discovery to application. Nature Materials. Nature Research; 2020;19:922-8. DOI: 10.1038/s41563-020-0778-5

[23] S. Radhakrishnan, C. Rao MV. Performance of Conducting Polyaniline-DBSA and Polyaniline-DBSA/Fe3O4 Composites as Electrode Materials for Aqueous Redox Supercapacitors. J Appl Polym Sci. 2011;122:1510-8. DOI: 10.1002/app.34236

[24] Li ZF, Zhang H, Liu Q, Liu Y, Stanciu L, Xie J. Covalently-grafted polyaniline on graphene oxide sheets for high performance electrochemical supercapacitors. Carbon. 2014;71:257-67. DOI: 10.1016/j.carbon.2014.01.037

[25] Eftekhari A, Li L, Yang Y. Polyaniline supercapacitors. J Power Sources. 2017;347:86-107. DOI: 10.1016/j.jpowsour.2017.02.054

[26] Alamin AA, Abd Elhamid AM, Anis WR, Attiya AM. Fabrication of symmetric supercapacitor based on relatively long lifetime polyaniline grown on reduced graphene oxide via Fe2+ oxidation sites. Diam Relat Mater. 2019;96:182-94.

[27] Li G, Zhang C, Li Y, Peng H, Chen K. Rapid polymerization initiated by redox initiator for the synthesis of polyaniline nanofibers. Polymer. 2010;51:1934-9. DOI: 10.1016/j.polymer.2010.03.004

[28] Odian G. Principles of polymerization. 4th ed. New Jersey: John Wiley & Sons; 2004. p. 216. DOI: 10.1002/047147875X

[29] Tawde S, Mukesh D, Yakhmi J V. Redox behavior of polyaniline as influenced by aromatic sulphonate

anions: Cyclic voltammetry and molecular modeling. Synth Met. 2002;125:401-13. DOI: 10.1016/S0379-6779(01)00483-0

[30] Jiang Q, Shang Y, Sun Y, Yang Y, Hou S, Zhang Y, et al. Flexible and multi-form solid-state supercapacitors based on polyaniline/graphene oxide/CNT composite films and fibers. Diam Relat Mater. 2019;92:198-207. DOI: 10.1016/j.diamond.2019.01.004

[31] P. Yu, X. Zhao, Z. Huang YL and QZ. Free-standing three-dimensional graphene and polyaniline nanowire arrays hybrid foams for high-performance flexible and lightweight supercapacitors. J Mater Chem A. 2014;4:14413-7. DOI: 10.1039/C4TA02721C

[32] Li D, Li Y, Feng Y, Hu W, Feng W. Hierarchical graphene oxide/polyaniline nanocomposites prepared by interfacial electrochemical polymerization for flexible solid-state supercapacitors. J Mater Chem A. 2015;3:2135-43. DOI: 10.1039/c4ta05643d

[33] Kalambate PK, Rawool CR, Karna SP, Srivastava AK. Nitrogen-doped graphene/palladium nanoparticles/porous polyaniline ternary composite as an efficient electrode material for high performance supercapacitor. Mater Sci Energy Technol. 2018;2:246-57. DOI: 10.1016/j.mset.2018.12.005

[34] He S, Hu X, Chen S, Hu H, Hanif M, Hou H. Needle-like polyaniline nanowires on graphite nanofibers: Hierarchical micro/nano-architecture for high performance supercapacitors. J Mater Chem. 2012;22:5114-20. DOI: 10.1039/c2jm15668g

[35] Dai W, Ma L, Gan M, Wang S, Sun X, Wang H, et al. Fabrication of sandwich nanostructure graphene/polyaniline hollow spheres composite and its applications as electrode materials for supercapacitor. Mater Res Bull. 2016;76:344-52. DOI: 10.1016/j.materresbull.2015.12.045

[36] Ning G, Li T, Yan J, Xu C, Wei T, Fan Z. Three-dimensional hybrid materials of fish scale-like polyaniline nanosheet arrays on graphene oxide and carbon nanotube for high-performance ultracapacitors. Carbon. 2013;54:241-8. DOI: 10.1016/j.carbon.2012.11.035

[37] S. Li, Ai. Gao, F.Yi, D. Shu, H. Cheng, Xi Zhou, C. He DZ and FZ. Preparation of carbon dots decorated graphene/polyaniline composites by supramolecular in-situ self-assembly for high-performance supercapacitors. Electrochim Acta. 2019;297:1094-103. DOI: 10.1016/j.electacta.2018.12.036

[38] Stoller MD, Ruoff RS. Best practice methods for determining an electrode material's performance for ultracapacitors. Energy Environ Sci. 2010;3:1294-301. DOI: 10.1039/c0ee00074d

[39] Railanmaa A, Kujala M, Keskinen J, Kololuoma T, Lupo D. Highly flexible and non-toxic natural polymer gel electrolyte for printed supercapacitors for IoT. Appl Phys A Mater Sci Process. 2019;125:168. DOI: 10.1007/s00339-019-2461-8

[40] Jian X, Yang H min, Li J gang, Zhang E hui, Cao L le, Liang Z hai. Flexible all-solid-state high-performance supercapacitor based on electrochemically synthesized carbon quantum dots/polypyrrole composite electrode. Electrochim Acta. 2017;228:483-93. DOI: 10.1016/j.electacta.2017.01.082

[41] Alipoori S, Mazinani S, Aboutalebi SH, Sharif F. Review of PVA-based gel polymer electrolytes in flexible solid-state supercapacitors: Opportunities and challenges. Journal of Energy Storage. 2020;27:101072. DOI: 10.1016/j.est.2019.101072

[42] Elhamid AM, Alamin AA, Selim AM, Wasfey MA, Zahran MB. Fabrication of Flexible, Half printed and All-Solid-State Symmetric Supercapacitor Based on Silver Decorated Reduced Graphene Oxide. In: ACCS/PEIT 2019 - 2019 6th International Conference on Advanced Control Circuits and Systems; Hurgada:IEEE: 2019. p. 151-5. DOI: 10.1109/ACCS-PEIT48329.2019.9062877

[43] Chen Q, Li X, Zang X, Cao Y, He Y, et al. Effect of different gel electrolytes on graphene- based solid-state supercapacitors. RSC Adv. 2014;36253:36253-6. DOI: 10.1039/c4ra05553e

[44] Yu C, An J, Chen Q, Zhou J, Huang W, Kim Y, et al. Recent Advances in Design of Flexible Electrodes for Miniaturized Supercapacitors. Small Methods. 2020;4:1900824. DOI: 10.1002/smtd.201900824

[45] Liu N, Gao Y. Recent Progress in Micro-Supercapacitors with In-Plane Interdigital Electrode Architecture. Small. 2017;13:1701989. DOI: 10.1002/smll.201701989

[46] Velasco A, Ryu YK, Boscá A, Ladrón-De-Guevara A, Hunt E, Zuo J, et al. Recent trends in graphene supercapacitors: From large area to microsupercapacitors Sustainable Energy and Fuels. 2021;5:1235-54. DOI: 10.1039/d0se01849j

[47] Ahmad H, Fan M, Hui D. Graphene oxide incorporated functional materials: A review. Coordination Chemistry Reviews. 2018;145:270-80. DOI: 10.1016/j.ccr.2017.03.021

[48] Kuila T, Mishra AK, Khanra P, Kim NH, Lee JH. Recent advances in the efficient reduction of graphene oxide and its application as energy storage electrode materials Nanoscale. 2013:5:52-71. DOI: 10.1039/c2nr32703a

[49] Kumar R, Singh RK, Singh DP, Joanni E, Yadav RM, Moshkalev SA. Laser-assisted synthesis, reduction and micro-patterning of graphene: Recent progress and applications. Coordination Chemistry Reviews. 2017;342:34-79. DOI: 10.1016/j.ccr.2017.03.021

[50] Thekkekara L V. Direct Laser Writing of Supercapacitors. In: Liudvinavičius L, editor. Supercapacitors - Theoretical and Practical Solutions. InTech; 2018. p. 103-16. DOI: 10.5772/intechopen.73000

[51] Okhrimchuk AG, Mezentsev VK, Schmitz H, Dubov M, Bennion I. Cascaded nonlinear absorption of femtosecond laser pulses in dielectrics. Laser Phys. 2009;19:1415-22. DOI: 10.1134/s1054660x09070081

[52] Arul R, Oosterbeek RN, Robertson J, Xu G, Jin J, Simpson MC. The mechanism of direct laser writing of graphene features into graphene oxide films involves photoreduction and thermally assisted structural rearrangement. Carbon. 2016;99:423-31. DOI: 10.1016/j.carbon.2015.12.038

[53] de Lima BS, Bernardi MIB, Mastelaro VR. Wavelength effect of ns-pulsed radiation on the reduction of graphene oxide. Appl Surf Sci. 2020;506:144808. DOI: 10.1016/j.apsusc.2019.144808

[54] Bhattacharjya D, Kim CH, Kim JH, You IK, In J Bin, Lee SM. Fast and controllable reduction of graphene oxide by low-cost CO 2 laser for supercapacitor application. Appl Surf Sci. 2018;462:353-61. DOI: 10.1016/j.apsusc.2018.08.089